Acta Oceanol. Sin., 2011, Vol. 30, No. 5, P. 23-32
DOI: 10.1007/s13131-011-0144-1
http://www.hyxb.org.cn
E-mail: hyxbe@263.net

Numerical study of M_2 internal tide generation and propagation in the Luzon Strait

LI Huan[1], SONG Dan[2], CHEN Xueen[3*], QIAN Hongbao[4], MU Lin[1], SONG Jun[1]

[1] National Marine Data and Information Service, State Oceanic Administration, Tianjin 300171, China

[2] Key Laboratory of Ocean Circulation and Waves, Institute of Oceanology, Chinese Academy of Sciences, Qingdao 266071, China

[3] College of Physical and Environmental Oceanography, Ocean University of China, Qingdao 266100, China

[4] Administrative Center for China's Agenda 21, Beijing 100038, China

Received 4 January 2011; accepted 14 June 2011

Abstract
Based on the *z*-coordinate ocean model HAMSOM, we introduced the internal-tide viscosity term and applied the model to numerically investigate the M2 internal tide generation and propagation in the Luzon Strait (LS). The results show that (1) in the upper 250 m depth, at the thermocline, the maximum amplitude of the generated internal tides in the LS can reach 40 m; (2) the major internal tides are generated to the northwest of Itbayat Island, the southwest of Batan Island and the northwest of the Babuyan Islands; (3) during the propagation the baroclinic energy scattering and reflection is obvious, which exists under the effect of the specific topography in the South China Sea (SCS); (4) the westward-propagating internal tides are divided into two branches entering the SCS. While passing through 118°E, the major branch is divided into two branches again. The strongest internal tides in the LS are generated to the northwest of Itbayat Island and propagate northeastward to the Pacific. However, to the east of 122°E, most of the internal tides propagate southeastward to the Pacific as a beam.

Key words: M_2 internal tides, HAMSOM, Internal tidal energy flux, Luzon Strait

1 Introduction

As a significant physical oceanographic phenomenon, internal tides play a key role in the dissipation of tidal energy and the balance of ocean energy budget. Internal tidal mixing has a positive effect on driving the thermohaline circulation in the ocean. In addition, the internal tides generated on the edge of the continental shelf can bring about upwelling, which is closely related to the transport of nutrients from the deep water to the shallow water. Currently, most of research on internal tide generation are based on the physical mechanism that the barotropic tidal current and topography interaction can generate the sustained periodic fluctuation in the stable stratification of seawater, which spreads all around and forms the internal tides eventually (Fang and Du, 2005; Vlasenko et al., 2010; Guo et al., 2011).

The Luzon Strait (LS) is to the northeast of the South China Sea (SCS), and between Luzon Island and Taiwan Island. As a primary passage connecting the SCS to the northwest Pacific, the LS is full of a large number of complex topography such as rough island slopes, deep trenches and prominent ridges. While the westward barotropic tides pass through the strait, the interaction between the barotropic tidal currents and those abruptly changing topography will generate a mass of strong internal tides. Therefore, as a desirable area, the strait is well selected to investigate and analyze the internal tide generation and propagation.

Recently, the major research on the internal tides in the LS and nearby regions is focused on observation analysis, satellite data analysis and numerical simulation. Based on four sets of ADCP measurements, Lien et al. (2005) confirmed that strong internal tides are generated in the LS, propagating as a narrow tidal

Foundation item: The Public Science and Technology Research Funds Projects of Ocean under contract Nos 200905001 and 201005019; the National Natural Science Foundation of China under contract No.41006002.
*Corresponding author, E-mail: xchen@ouc.edu.cn

beam into the SCS, which are amplified by the shoaling continental slope near the Dongsha Islands, and become nonlinear and evolve into high-frequency nonlinear internal waves. Yang (2008) used the baroclinic velocity extracted from LADCP measurements to calculate an internal tidal energy flux in the LS and demonstrated that an internal tidal energy which spreads to the SCS is stronger than that spread to the Pacific. Moreover, in the diurnal and semidiurnal internal tidal energy there exist seasonal differences obviously. Gao et al. (2010) based on the CTD data obtained from 4 repeatedly observed stations located at 19.5°–21.0°N, 121°E, in the LS, discussed a role of disturbances caused by the internal tides in temperature and salinity profiles in calculating the geostrophic currents. Based on the analysis of SAR images, Shen and He (2006) confirmed that the internal waves generated to the north of the SCS propagate a long distance with unchanged wave form, and mainly come from the LS. Compared with observation and satellite data analysis, the numerical simulation is mostly adopted to the investigation of the internal tides in the LS. Niwa and Hibiya (2004) used POM to investigate the energy flux of the M_2 internal tides around the continental shelf edge in the East China Sea and confirmed that the M_2 internal tides in the northwest Pacific are effectively generated over prominent topographies such as the subsurface ridges in the LS. Based on POM, Wu (2006) established a three-dimensional (barotropic tides and baroclinic tides) tidal wave assimilation model to simulate the M_2 internal tides generated in the LS. The results suggest that most of the internal tides propagate westward on the SCS continental shelf and gradually evolve into the high-frequency internal waves under the nonlinear effect of topography. Currently, governing equations in most of the z-coordinate numerical ocean models depend on hydrostatic assumptions and various physical approximations such as the linear approximation, thus the evolution and energy dissipation of internal tides during their propagation cannot be well simulated. Song et al. (2010) introduced the internal-tide viscosity (ITV) term into a z-coordinate ocean model to simulate the instantaneous isopycnal vertical displacements at the 1 000 m depth in the LS and the results well reproduce the propagation of the M_2 internal tides in the LS and nearby regions.

In this paper, we use a parameterization scheme suggested by Song et al. (2010) and introduce the ITV term into the z-coordinate ocean model HAMSOM to further investigate M_2 internal tide generation and propagation in the LS.

2 Internal-tide viscosity term

Owing to the step-like representation in a z-coordinate system, a rough topography looks mostly like a "wall" rather than a sloping bottom. Therefore, to maintain the continuity of incompressible seawater, horizontally back and forth tidal currents over the rough topography are reproduced into vertical oscillations alongside the "wall". The turbulent bottom layer (TBL) which should be attached to the sloping bottom also disappears because of the wall-like reconstruction. If the dissipative effect of seawater viscidity in modeling the vertical motion of internal tides is unconsidered, the dissipation occurring in the TBL in those special regions over rough topography will not be well simulated (Song et al., 2010). In addition, in the stratified ocean interior, where the strongest internal tide oscillation occurs, the energy dissipation during their propagation, including multiscale energy transfer processes such as nonlinear wave-wave and wave-current interactions, should not be ignored (Fang and Du, 2005). Considering the features of internal tide oscillation, which can vertically govern the entire water column with the strongest of which occurring in the interior where the most intense density stratification is located, Song et al. (2010) confirmed that an significant numerical closure scheme that estimates the internal tidal energy loss during the propagation is missing in primitive equation ocean models. To further modify the numerical closure scheme, the vertical momentum equilibrium in the viscous seawater is rethought and the horizontal viscosity term referred to as the internal tidal viscosity (ITV) term is retained in the vertical motion equation. The introduction of the internal tidal viscosity term to z-coordinate ocean model leads to significant improvements, not only for the simulated vertical motion of internal tides, but also for the dissipation of barotropic tides and the modeled vertical temperature structure. The most important effect of seawater viscidity on internal tide oscillation, is that on one hand it increases the local dissipation in areas over the rough topography in a z-coordinate system, on the other hand it converts internal tide propagation into a more reasonable dissipative mode. The specific parameterization scheme can be found in Song et al. (2010).

3 Model descriptions

A three-dimensional z-coordinate ocean model, Hamburg shelf ocean model (HAMSOM), is adopted in our research, which is developed by Backhaus et al. (1985) and has been widely used in Europe for 20 a The numerical schemes of the model have been described in detail by Backhaus (1985).

In this paper, the model domain covers 16°–23°N, 110°–125°E (Fig.1), and the bathymetric data are extracted from the general bathymetric chart of the oceans (GEBCO) global bathymetric data. Generally, the horizontal wavelength of large-scale M_2 internal tides can reach 150–200 km, and that of small-scale ones also can reach several kilometers, therefore, the $2' \times 2'$ horizontal resolution is adopted to the model effectively. Since the stratification deeper than 5 500 m has little influence on our research, we set the depth more than 5 500 m to be 5 500 m, and divide the water column into 32 layers.

Model runs are forced by the tidal elevation on all open boundaries. The tidal elevation is extracted from the TPXO 7.1, which is from a high-quality inverse model of the barotropic tides (Egbert and Erofeeva, 2002). The initial field of the model is extracted from the simple ocean data assimilation (SODA) data set (Carton et al., 2000 a,b) and interpolated to the corresponding model grid. In addition, as velocity open boundary conditions, the Orlanski radiation boundary conditions are selected. It should be mentioned that since the barotropic tidal current and topography interaction is the major generating mechanism for the internal tides, the impact of sea surface pressure, wind stress and heat flux is not considered in the model. We set the initial time to 00:00 1 January 2001 and use 2 min time-step to run the model. In the 60 d running period, we select the hourly model results of the final 15 d to analyze, and use the previous 45 d to steady the model.

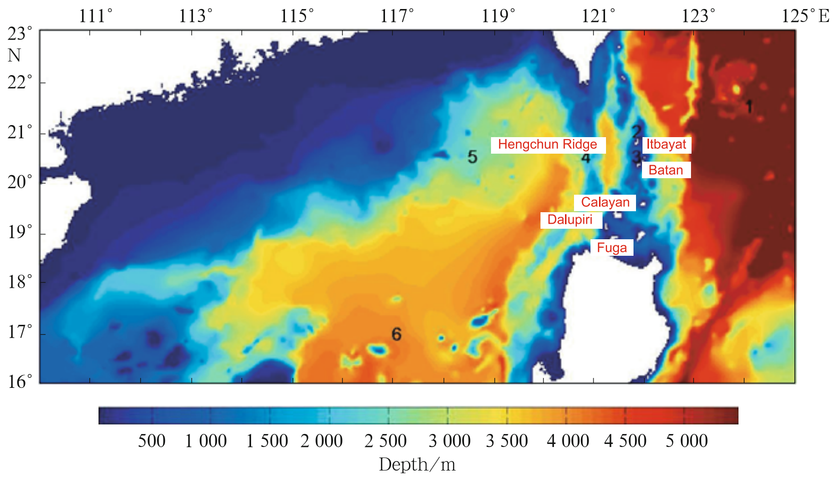

Fig.1. The topography of the model.

Table 1. The thickness per layer

Layer	1–3	4	5–8	9–11	12–23	24–25	26–32
Thickness/m	10	20	25	50	100	250	500

4 Results

4.1 *M_2 tide*

Associating with the physical mechanism of the barotropic tidal current and topography interaction, the internal tides are generated under the impact of barotropic tides, and therefore, the accuracy of the internal tides can be identified by the accuracy of the barotropic tide in the model.

In this paper, the simulated M_2 tidal constituent cotidal charts are shown and compared with the TPXO 7.1 results in Fig.2. The left part of the figure is the modeled results, and the right part is the TPXO 7.1 results. The corresponding charts compared with each other illustrate that the modeled results agree with the TPXO 7.1 results very well. As shown in Fig.2, the amplitude of the M_2 barotropic tide from the Pacific can reach 0.4–0.6 m, but in most regions of the SCS, it is less than 0.3 m. when the westward M_2 barotropic tide passes through the Luzon Strait, it is divided into two major branches–the southwestward-propagating branch and the northwestward-propagating branch along Taiwan Island. While the two branches propagate in the SCS, the tidal amplitude is gradually increasing on the continental shelf with the nonlinear effect of the shoaling topography, and even can reach more than 0.8 m. It is worth notice that in the model results some large-scale ripples appear on the sea surface around the LS, but in the TPXO 7.1 results, the ripples are not discernible because of the smooth contour lines. This comparison indicates that in the model the generated internal tides have a obvious modulation to the amplitude and phase of the barotropic tide, which makes the original contour lines of amplitude and phase appear with varying curves (Jan et al., 2007).

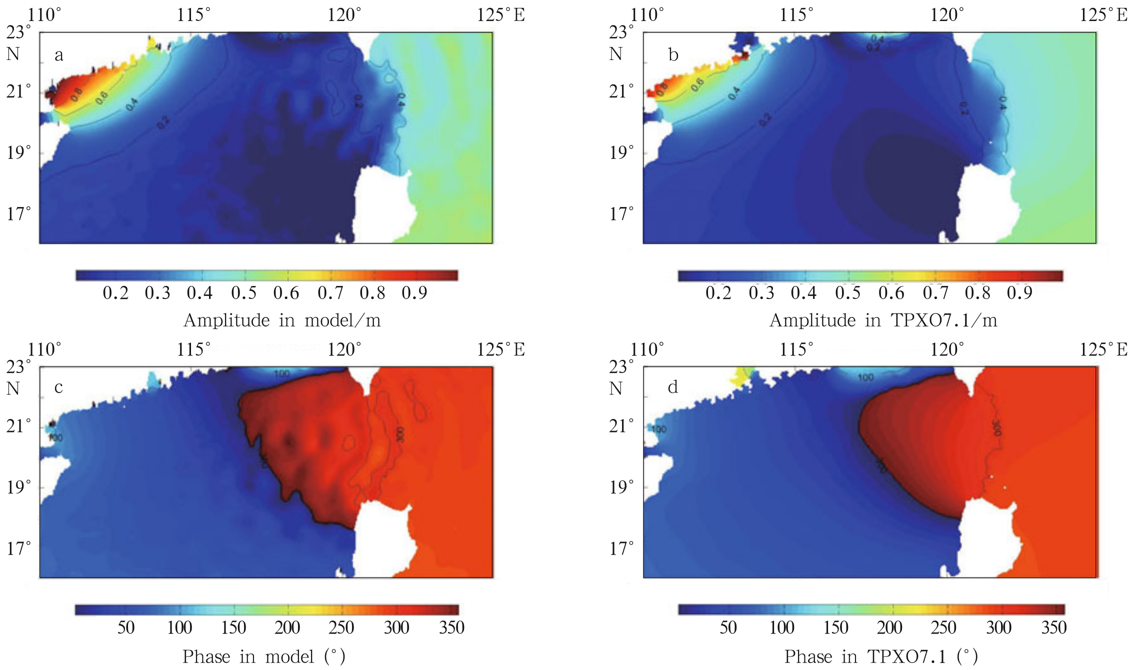

Fig.2. The M_2 tidal constituent cotidal charts.

To further validate the modeled results, the root-mean-square (RMS) difference (Cummins and Oey, 1997) is adopted:

$$E = \sqrt{\frac{1}{2}(A_{\rm o}^2 + A_{\rm m}^2) - A_{\rm o}A_{\rm m}\cos(\varphi_{\rm o} - \varphi_{\rm m})}, \qquad (1)$$

where A is the amplitude; φ is the phase; the subscript m is for the modeled results; and the subscript o is for the TPXO 7.1 results. The distribution of RMS difference is shown in Fig.3. In the figure, 78.25% of the RMS difference in the whole region is less than 0.05 m, but in the LS and nearby regions, the RMS difference is high (0.05–0.1 m). To the south of the Taiwan Strait and the South China coast, the RMS difference is higher, and even can reach more than 0.25 m. In order to give a further explanation, Fig.4 displays the distribution of the tidal amplitude difference between the modeled results and the TPXO 7.1 results. In Fig.4, the regions full of high amplitude difference well agree with the high RMS difference distribution (Fig.3), thus it can be concluded that the high RMS difference mainly stems from the amplitude difference between the modeled results and the TPXO 7.1 results. In the LS, the modulation effect of the simulated underlying internal tides changes the original amplitude of the barotropic tide so that the amplitude difference is higher. However, the higher amplitude difference near the coast indicates that during the propagation the barotropic tidal energy loss under the nonlinear effect of the shoaling topography is hard to be well simulated in the model. Some reasons such as the precision of the shoaling topography maybe result in this difference. In this paper, however, we majorly focus on the investigation of the internal tides in the LS, and the influence of the RMS difference close to the coast will not be considered.

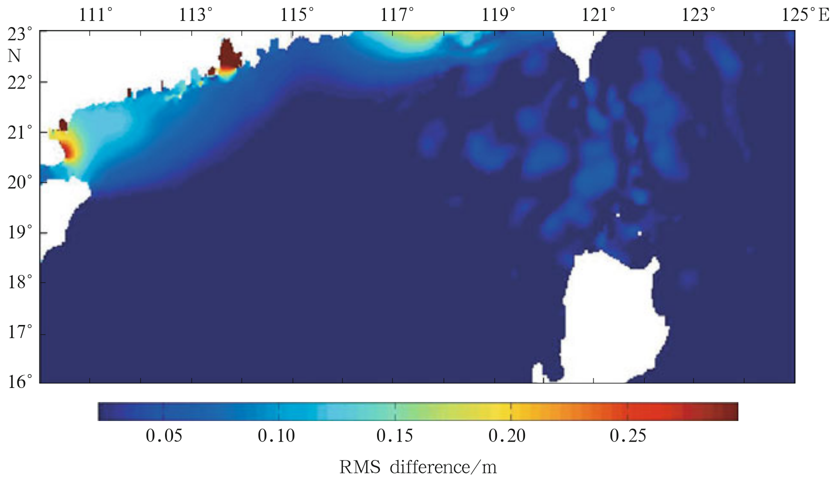

Fig.3. The RMS difference distribution in the whole region.

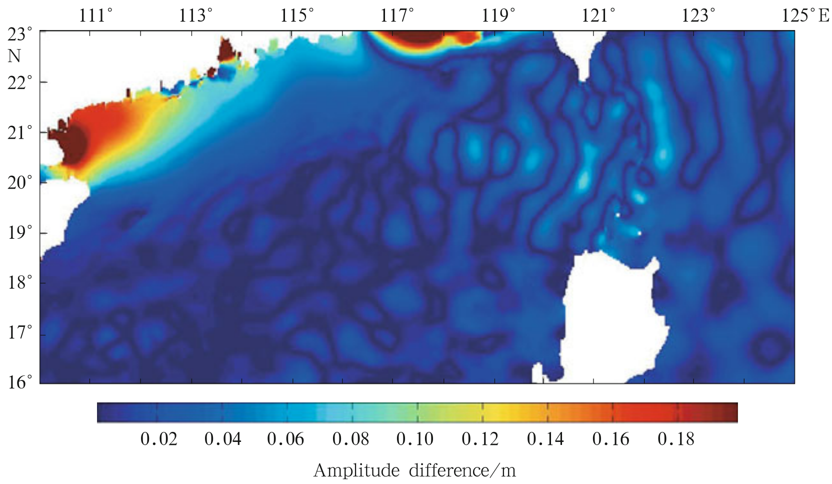

Fig.4. The difference in the tidal amplitude between the modeled results and the TPXO 7.1 results.

4.2 *M_2 internal tides*

Generally, the internal tides can be characterized by a vertical isotherm fluctuation. Therefore, six points are selected respectively to display the vertical isotherm fluctuation in the upper 250 m (Fig.5). Table 2 shows the specific location and depth of each point. In Fig.5, according to the time series charts, the fluctuation of the vertical isotherm at all points indicates that the period of internal tides well agrees with that of M_2 barotropic tide. It also can be seen clearly that at Points 2–5 all of the maximum internal tide amplitudes are at the thermocline but different with each other. For example, at Point 2, 35 m maximum amplitude exists in 150–220 m; at Point 3, 40 m maximum amplitudes exists in 150–230 m; at Point 4, 30 m maximum amplitudes exists in 170–210 m; and at Point 5, 20 m maximum amplitude exists in 150–190 m. Obviously, the internal tide intensity at Points 2–4 is higher. According to Table 2, those points are close to the island slopes, where the interaction between large numbers of barotropic tidal currents and abruptly changing topography majorly contributes to the local internal tide generation. It should be mentioned that, as we can see from Fig.5 and Table 2, Points 1 and 6, where the internal tides exist with very low intensity, are selected respectively from the ocean and deep sea, moreover, adopting the mechanism of the barotropic tidal current and topography interaction to explain the internal tide generation in the ocean and deep sea is extremely controversial so that another different viewpoints such as the effect of the vertical component of tidal generation force, Coriolis resonance interaction and so on were referred (Du et al., 2001), thus in this paper, considering the uncertainty of the physical mechanism of the internal

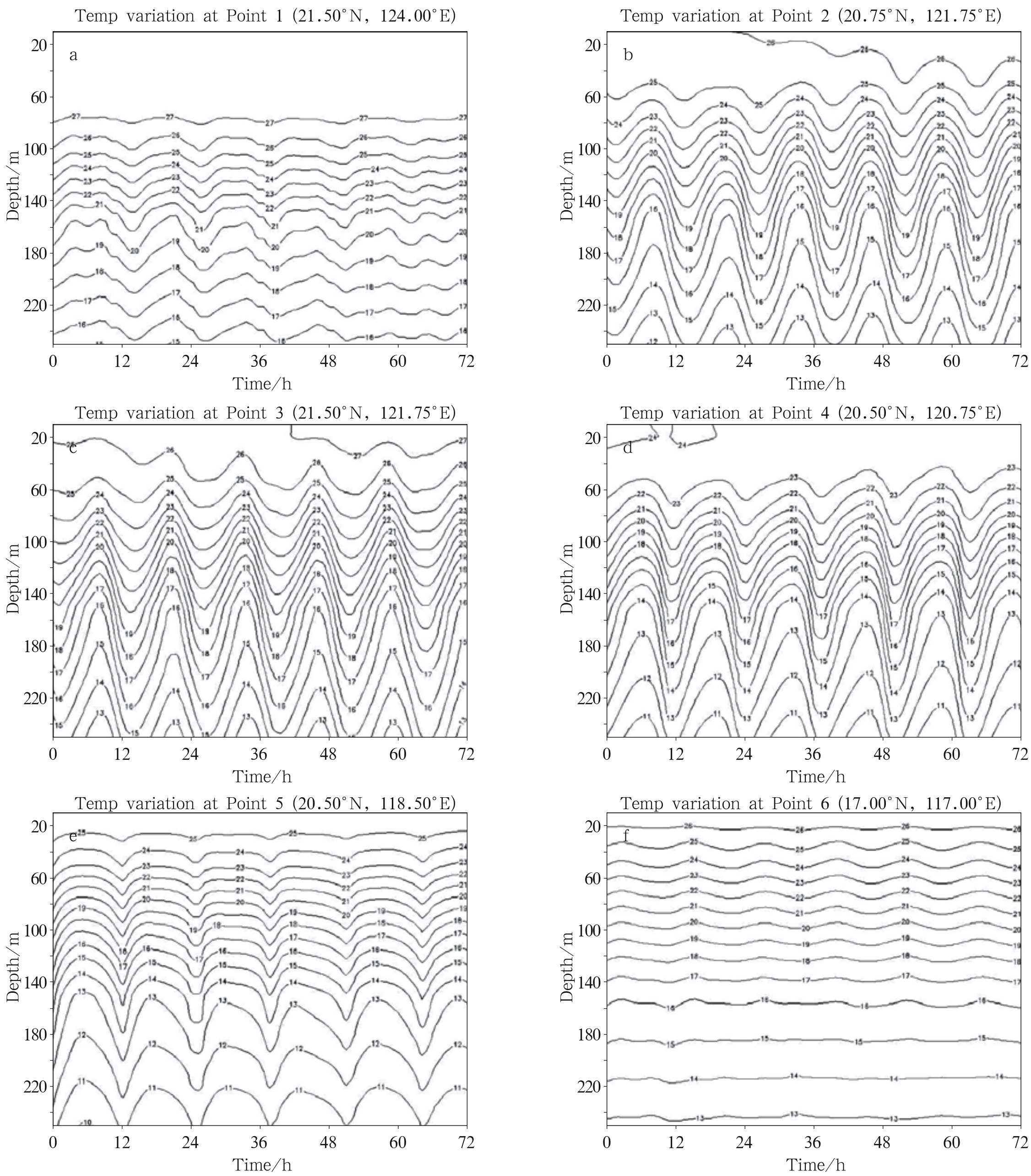

Fig.5. The vertical isotherm fluctuation in the upper 250 m at each point.

Table 2. The specific information of each point

Point	North latitude (°)	East longitude (°)	Depth/m	Location
1	21.50°	124.00°	4 976	in the Pacific
2	20.75°	121.75°	665	to the northwest of Itbayat Island
3	20.50°	121.75°	695	to the northwest of Batan Island
4	20.50°	120.75°	2 536	to the west of the Hengchun Ridge
5	20.50°	118.50°	2 476	on the slope to the west of the LS
6	17.00°	117.00°	3 984	in the SCS

tide generation in the ocean and deep sea, we will not investigate the internal tides at Points 1 and 6 in detail. But we can confirm that due to the propagation characteristics of internal tides, actually the internal tides at Points 1 and 6 should include a part of those generated in the LS.

4.3 *The internal tidal (baroclinic) energy flux in the LS*

To calculate the baroclinic energy flux, the method from Nash et al.(2005) is adopted.

First of all, we use the method of thickness-weighted average to extract the barotropic velocity from the total velocity:

$$\overline{u} = \frac{1}{\sum\limits_{n=1}^{k} h_n} \sum_{n=1}^{k} h_n u_n, \tag{2}$$

where k is the total number of layers; n is the nth layer; h is the thickness per layer; and the perturbation velocity is defined as follows:

$$u_n' = u_n - \overline{u}. \tag{3}$$

Then the perturbation pressure is calculated:

$$p'(z,t) = p_{\rm s}(t) + \int_z^0 \rho'(\widehat{z},t) g d\widehat{z}. \tag{4}$$

Although the baroclinic-induced surface pressure $p_{\rm s}(t)$ is not measured, it can be inferred from the baroclinicity condition that the depth-averaged pressure perturbation must vanish:

$$\frac{1}{H}\int_{-H}^{0} p'(\widehat{z},t) dz = 0, \tag{5}$$

where $\rho'(\widehat{z},t)$ is the perturbation density, as in the following formula:

$$\rho'(\widehat{z},t) = \rho(z,t) - \overline{\rho}(z), \tag{6}$$

where $\rho(z,t)$ is the instantaneous density; and $\overline{\rho}(z)$ is the time-mean vertical density profile, averaged over at least one wave period (>12.4 h).

If $p_{\rm s}$ and $\rho'(\widehat{z},t)$ are determined, we can obtain the perturbation pressure $p'(z,t)$ and calculate the baroclinic energy flux:

$$F = \sum_{n=1}^{k} u_n' h_n p_n'. \tag{7}$$

According to the Eqs (4)–(7), a instantaneous zonal distribution of baroclinic energy flux is shown in Fig.6. It can be seen that most of the strong baroclinic energy concentrate in the middle of the strait. Between 121.0° and 121.5°E, where the Hengchun Ridge, the Luzon Trench and the Luzon island arc constitute the major topography of the strait, the westward energy exceeds that in another region in intensity. However, compared with the strong westward energy, most of the strong eastward energy concentrate around the Luzon island arc, especially to the northwest of Itbayat Island, southwest of Batan Island, and the northwest of the Babuyan Islands.

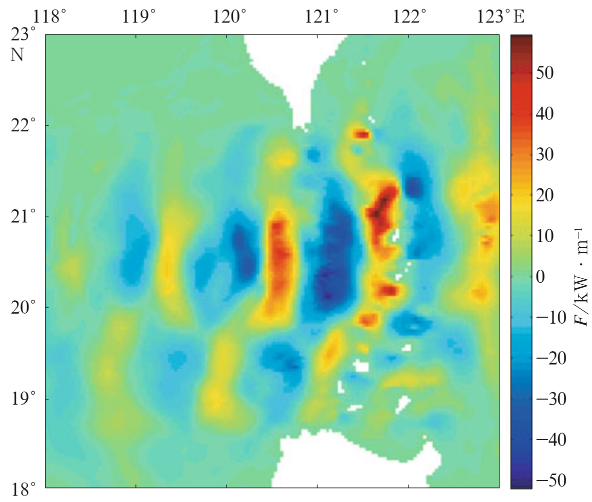

Fig.6. The instantaneous zonal distribution of the baroclinic energy flux in the LS.

Considering the baroclinic energy can be characterized by the horizontal baroclinic velocity, an instantaneous vertical section of horizontal baroclinic velocity is shown in Fig.7. The distribution of the baroclinic velocity at the 20.5°N section illustrates that the extremely strong westward baroclinic velocity near Batan Island is concentrated on the leading edge of the island, extending obliquely downward to the Hengchun Ridge. But on the top of the ridge, the distribution of baroclinic velocity presents an obvious change that a

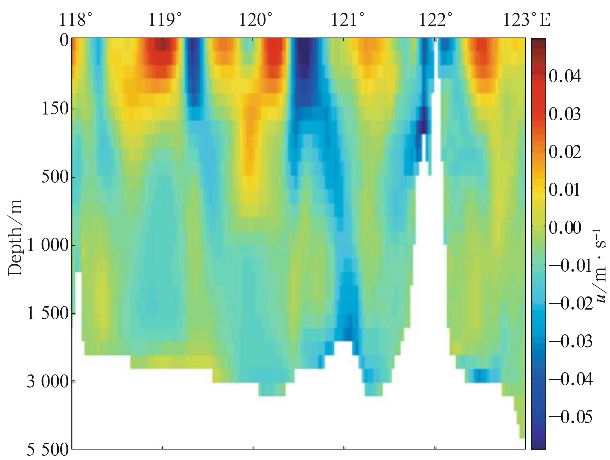

Fig.7. The distribution of the instantaneous baroclinic velocity at the 20.5°N section.

discernible beam-like velocity structure appears with extending obliquely upward to the sea surface. The similar phenomenon such as the beam-like velocity structure is illustrated by Niwa and Hibiya (2004) (Fig.8). Combining with some research on the internal tide scattering on rigdes and islands (Johnston and Merrifield, 2003), we can conclude that on the leading edge of Batan Island, the westward baroclinic energy scatters under the effect of supercritical topography and propagates obliquely downward along ray-like paths, while on the Hengchun Ridge, under the effect of supercritical and near-critical topography, the energy reflects and extends to the sea surface along curved ray-like paths in the realistic stratification. Moreover, while arriving at the sea surface, the energy reflects again. It should be mentioned that to the west of the Hengchun Ridge the westward-propagating energy beam is gradually broadened and weakened during the continuous reflection between the bottom and the surface. Associating with Johnston and Merrifield's (2003), research, we can also conclude that in the lee of the Hengchun Ridge, the internal tides form different modes which interfere with each other, thus the wave-wave interference broadens and weakens the propagating energy beam.

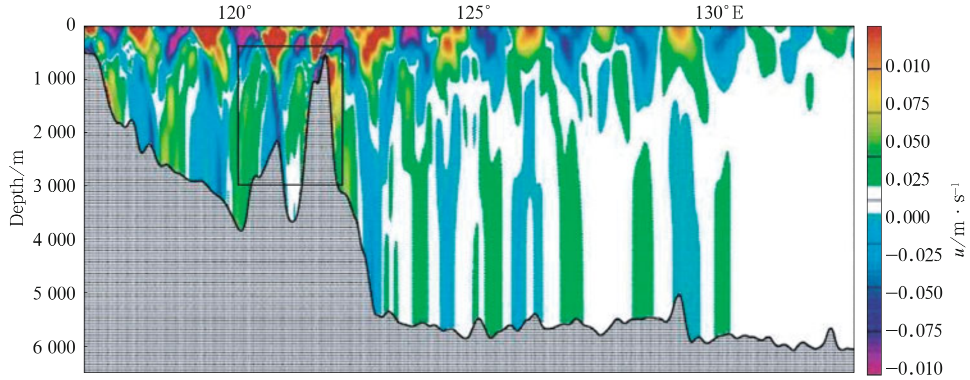

Fig.8. The distribution of the instantaneous baroclinic velocity at the 21.5°N section [from Niwa and Hibiya (2004)].

4.4 *Internal tide generation sites*

To identify internal tide generation sites, a divergence distribution of the depth-integrated baroclinic energy flux is given in Fig.9.

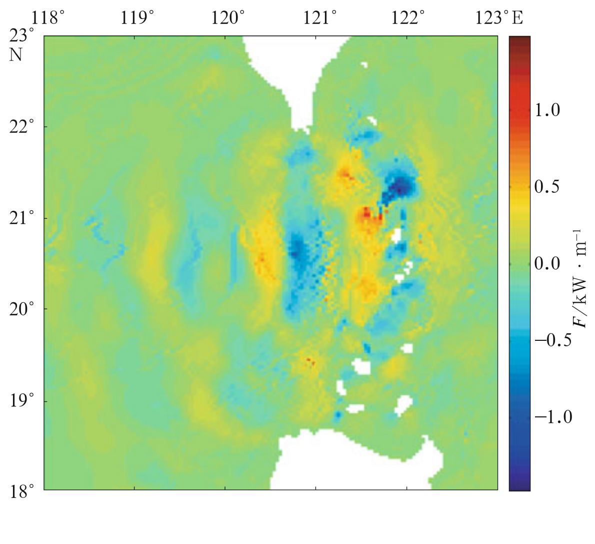

Fig.9. The divergence distribution of the baroclinic energy in the LS.

The divergence is in accordance with the following equation:

$$\mathrm{div}F = \frac{\partial F_x}{\partial x} + \frac{\partial F_y}{\partial y}, \quad (8)$$

where F_x is the baroclinic energy flux in the x direction; and F_y is that in the y direction. In this paper, we use the average energy flux extracted from the modeled results of the final 2 d to calculate the divergence.

In Fig.9, most of high positive divergence concentrate to the northwest of Itbayat Island, the southwest of Batan Island, the northwest of the Babuyan Islands as well as the west of the Hengchun Ridge. The distribution of the high positive divergence indicates that most of internal tides are majorly generated in those regions. We can note that since the baroclinic energy generated from the Luzon island arc propagates westward to the SCS, the internal tides near the Hengchun Ridge should include two parts–those generated under the interaction between the local barotropic tide currents and the topography, and those generated near the Luzon island arc. Figure 10 is the major generation sites concluded from some MODIS images (Wu, 2008), it can be seen that those sites agree with the modeled results very well. In addition, associating with Holloway's (2001), viewpoint that baroclinic energy generation and dissipation regions are adjacent, we can see that near the regions full of strong positive divergence, the negative-divergence parts which indicate the energy dissipation are also discernible.

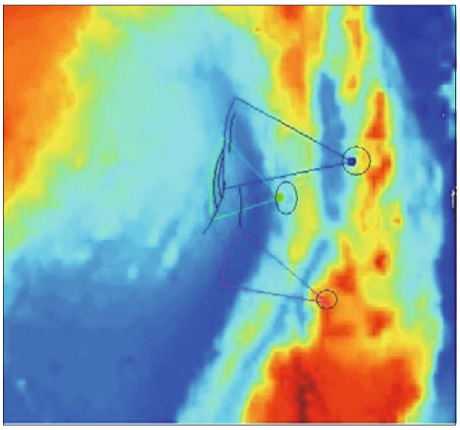

Fig.10. The major internal wave generation sites concluded from some MODIS images [from Wu (2008)].

4.5 *Internal tide propagation*

Figure 11 shows that the propagation of the baroclinic energy generated in the LS, and the average energy is extracted from the modeled results of the final 2 d. In the figure, the energy less than 3 kW/m is filtered in order to make the distribution and propagation paths of the generated internal tides more discernible. Between 121° and 121.5°E, where strong internal tides are divided into two branches propagating to the SCS, one branch generated to the northwest of the Babuyan Islands turns to the southwest entering the SCS Basin directly, and the other generated near Itbayat Island and Batan Island is the major branch which propagates westward to the continental shelf as a beam. While passing through 118°E, the major one is divided into two branches again, as shown in the figure, a part of the internal tides forms one branch and turns to the southwest entering the SCS Basin, and the other turns to the northwest propagating towards the South China coast. Combing with the propagation features of the barotropic tide that passes through the LS and enters the SCS (Fig.2), we can conclude that the propagation paths of the westward internal tides are determined by the propagation paths of the barotropic tide and the topography of the SCS including the deep basin and the continental. Owing to the ITV term introduced into the model the baroclinic energy loss near the continental shelf is extremely notable, in other words, the step-like sloping topography in the SCS has real energy dissipation effect so that the distribution of the simulated energy is more reasonable. In addition, in the figure the strongest internal tides in the LS are generated to the northwest of Itbayat Island and propagate northeastward to the Pacific, which can reach more than 45 kW/m. However, to the east of 122°E, most of the internal tides propagate southeastward to the Pacific as a beam.

5 Conclusions

Based on the z-coordinate model HAMSOM, we introduced the internal-tide viscosity term and applied the modified model to investigate the M_2 internal tides in the LS for its generation and propagation.

(1) In the upper 250 m depth, at the thermocline, the maximum amplitude of the generated internal tides in the LS can reach 40 m.

(2) The major internal tides are generated to the northwest of Itbayat Island, the southwest of Batan Island and the northwest of the Babuyan Islands.

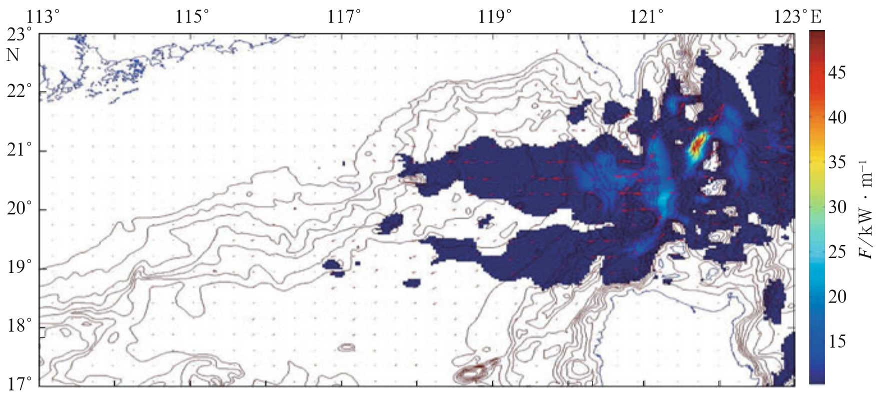

Fig.11. The internal tide propagation.

(3) On the leading edge of Batan Island, the westward baroclinic energy scatters under the effect of supercritical topography and propagates obliquely downward along ray-like paths, while on the Hengchun Ridge, under the effect of supercritical and near-critical topography, the energy reflects and extends to the sea surface along curved ray-like paths in the realistic stratification. Moreover, while arriving at the sea surface, the energy reflects again. In addition, in the lee of the Hengchun Ridge, the internal tides form different modes which interfere with each other, thus the wave-wave interference broadens and weakens the propagating energy beam.

(4) The westward-propagating internal tides are divided into two branches entering the SCS. While passing through 118°E, the major branch is divided into two branches again. The propagation paths of the westward internal tides are determined by the propagation paths of the barotropic tide and the topography of the SCS including the deep basin and the continental shelf. The strongest internal tides in the LS are generated to the northwest of Itbayat Island and propagate northeastward to the Pacific. However, to the east of 122°E, most of the internal tides propagate southeastward to the Pacific as a beam.

Acknowledgements

The authors thank two anonymous reviewers whose comments are valuable and have greatly improved the paper.

References

Backhaus J O. 1985. A three-dimensional model for the simulation of shelf sea dynamics. Ocean Dynamics, 38(4): 165–187

Carton J A, Chepurin G, Cao X. 2000a. A simple ocean data assimilation analysis of the global upper ocean 1950–1995: Part II. Results. Journal of Physical Oceanography, 30(2): 311–326

Carton J A, Chepurin G, Cao X, et al. 2000b. A simple ocean data assimilation analysis of the global upper ocean 1950–95: Part I. Methodology. Journal of Physical Oceanography, 30(2): 294–309

Cummins P, Oey L. 1997. Simulation of barotropic and baroclinic tides off northern British Columbia. Journal of Physical Oceanography, 27: 762–781

Du Tao, Wu Wei, Fang Xinhua. 2001. The generation and distribution of ocean internal waves. Marine Sciences (in Chinese), 25(4): 25–27

Egbert G D, Erofeeva S Y. 2002. Efficient inverse modeling of barotropic ocean tides. Journal of Atmospheric and Oceanic Technology, 19(2): 183–204

Fang Xinhua, Du Tao. 2005. Fundamentals of Oceanic Internal Waves and Internal Waves in the China Seas (in Chinese). Qingdao: China Ocean University Press, 337

Gao Kun, Chen Xueen, et al. 2010. The influence of internal tide on the diagnostic calculation of geostrophic current in Luzon Strait. Periodical of Ocean University of China (in Chinese), 40(2): 9–16

Guo Chuncheng, Chen Xueen, Vlasenko V, et al. 2011. Numerical investigation of internal solitary waves from the Luzon Strait: Generation process, mechanism and three-dimensional effects. Ocean Modelling, 38: 203–216

Holloway P E. 2001. A regional model for the semidiurnal tide on the Australian north west shelf. Journal of Geophysical Research, 106: 19625–19637

Jan S, Chern C S, Wang J, et al. 2007. Generation of diurnal K_1 internal tide in the Luzon Strait and its influence on surface tide in the South China Sea. Journal of Geophysical Research, 112: C06019, doi: 10.1029/2006JC004003

Johnston T M S, Merrifield M A. 2003. Internal tide scattering at seamounts, ridges, and islands. Journal of Geophysical Research, 108(C6): 3180, doi:10.1029/2002JC001528

Lien R C, Tang T Y, Chang M H, et al. 2005. Energy of nonlinear internal waves in the South China Sea. Geophysical Research Letters, 32: L05615, doi: 10.1029/2004GL22012

Nash J D, Kunze E, Toole J M, et al. 2005. Structure of the Baroclinic Tide Generated at Kaena Ridge, Hawaii. Journal of Physical Oceanography, 36: 1123–1135

Niwa Y, Hibiya T. 2004. Three-dimensional numerical simulation of M_2 internal tides in the East China Sea. Journal of Geophysical Research, 109: C04027, doi: 10.1029/2003JC001923

Shen Hui, He Yijun. 2006. SAR imaging simulation of horizontal fully two-dimensional internal waves. Journal of Hydrodynamics, 18(3): 294–302

Song Dan, Thomas P, Chen Xueen, et al. 2010. The role of seawater viscidity in modeling the vertical movement of internal tides. Ocean Modelling, 34(3–4): 63–69, doi: 10.1016/j.ocemod.2010.04.005

Vlasenko V, Stashchuk N, Guo C, et al. 2010. Multimodal structure of baroclinic tides in the South China Sea, Nonlin. Processes Geophys, 17: 529–543

Wu Ruizhong. 2008. A Numerical Study on Internal Wave Generate by Tidal Motion in the Luzon Strait (in Chinese). Taiwan: National Sun Yat-sen University Press

Wu Ziku. 2005. The Study of the Internal Tide 3-D Numerical Simulation with Assimilation in the South China Sea (in Chinese). Qingdao: Ocean University of China Press

Yang Qingxuan. 2008. Study on the Fluxes in the Luzon Strait and Turbulent Mixing in the South China Sea (in Chinese). Qingdao: Ocean University of China Press